Evidence that CED-9/Bcl2 and CED-4/Apaf-1 localization is not consistent with the current model for *C. elegans* apoptosis induction

Ehsan Pourkarimi[1], Sebastian Greiss[1, 2], Anton Gartner[1]

[1]Wellcome Trust Centre for Gene Regulation and Expression, University of Dundee, Dundee DD1 5EH, UK

[2]Current address: MRC Laboratory of Molecular Biology, Cambridge CB2 0QH, UK

Correspondence: Anton Gartner, Email: a.gartner@dundee.ac.uk , Phone: +44 1382 385809

Authors: Ehsan Pourkarimi, Email: e.pourkarimi@dundee.ac.uk

Sebastian Greiss, Email: sgreiss@mrc-lmb.cam.ac.uk

Key Words: *CED-4, Apaf-1, CED-9, Bcl-2, C. elegans*, apoptosis

Running Title: Localization of *C. elegans* apoptosis proteins

Abstract

In *C. elegans* the BH3-only domain protein EGL-1, the Apaf-1 homolog CED-4 and the CED-3 caspase are required for apoptosis induction while the Bcl-2 homolog CED-9 prevents apoptosis. Mammalian Bcl-2 inhibits apoptosis by preventing the release of the Apaf-1 activator cytochome c from mitochondria. In contrast *C. elegans* CED-9 is thought to inhibit CED-4 by sequestering it at the outer mitochondrial membrane by direct binding. We show that CED-9 associates with the outer mitochondrial membrane within distinct foci that do not overlap with CED-4, which is predominantly perinuclear and does not localize to mitochondria. CED-4 further accumulates in the perinuclear space in response to proapoptotic stimuli such as ionizing radiation. This increased accumulation depends on EGL-1 and is abrogated in *ced-9* gain-of-function mutants. CED-4 accumulation is not sufficient to trigger apoptosis execution, even though it may prime cells for apoptosis. Our results suggest that the cell death protection conferred by CED-9 cannot be solely explained by a direct interaction with CED-4.

Introduction

Seminal studies on *C. elegans* apoptosis that occurs during the invariant development of the worm were important for our general understanding of the mechanism of apoptosis induction. EGL-1, CED-4 and CED-3 are conserved proteins required for the vast majority of the 131 cell deaths that occur during nematode development [1] [2] [3]. The sole nematode Bcl2 family member CED-9 is required to protect healthy cells from undergoing apoptosis [3]. *ced-9* loss-of-function mutants undergo inappropriate apoptosis in cells that are normally destined to survive, while a *ced-9* gain-of-function mutant is defective for apoptosis induction in cells normally destined to die [3]. In the worm, apoptosis generally involves the transcriptional up-regulation of the BH3-only domain protein EGL-1, mediated by a combination of transcriptional regulators acting on *egl-1* in the specific cells destined to die [2] [4]. EGL-1 antagonizes CED-9, which in turn antagonizes the pro-apoptotic activity of CED-4, the Apaf1 homolog [2] [4]. In contrast to mammalian systems where Apaf-1 activation is linked to the release of cytochrome c from mitochondria [5], in *C. elegans* the decision between the survival or the death of a cell is reported to be largely regulated by the direct interaction of CED-4 and CED-9 [6]. Mitochondrial CED-9 directly binds pro-apoptotic CED-4 to inhibit apoptosis induction in cells destined to survive. Upon transcriptional induction, EGL-1 binding to CED-9 leads to a conformational change in CED-9 resulting in the release of CED-4 and its translocation to the nuclear periphery [6]. This event leads to CED-4 oligomerization and the induction of apoptosis through CED-3 caspase activation [7] [8] [6]. Recent structural evidence suggests that the activated CED-4 complex is comprised of a funnel-like octameric structure with 4-fold symmetry, each unit being defined by an asymmetric CED-4 dimer [9]. The cavity of this structure provides space for a CED-3

dimer, and the induced proximity of these two CED-3 molecules is likely to be required for caspase activation [9]. The notion that EGL-1/CED-9 and CED-9/CED-4 can directly interact is supported by yeast two-hybrid analysis, by co-immunoprecipitation studies in heterologous systems, and by crystallographic evidence showing that CED-9 can bind to a CED-4 dimer [10] [11] [8] [12] [9]. Previous cytological studies in *C. elegans* embryos appeared to show the colocalization of CED-9 and CED-4 on mitochondria in non-apoptotic cells, and indicated that CED-4 translocation to the perinuclear space was linked to apoptosis induction [6]. While there is no evidence for cytochorme c release in *C. elegans*, the release of other mitochondrial factors such AIF and EndoG as well as mitochondrial fragmentation has been implicated in apoptosis induction [13] [14]. However, the apoptosis defective phenotypes associated with the depletion of these factors are very weak and the importance of mitochondrial fragmentation has been debated [13] [14]. Furthermore, there is evidence that CED-9 permeabilizes membranes in vitro and the overexpression of CED-9 and Bcl-2 has been shown to lead to mitochondrial fusion in mammalian tissue culture and in *C. elegans* [15] [16] [17]. Here we revisit the localization of CED-9 and CED-4. We confirm that CED-9 is located at mitochondria and show that it forms distinct foci. Unexpectedly, CED-4 does not localize at mitochondria in the germ line and we provide strong evidence that this is also the case during somatic development. Using the *C. elegans* germ line as a model we show that CED-4 perinuculear accumulation might prime cells for apoptosis induction but is not sufficient to induce apoptosis.

Results

We previously generated two specific CED-4 antibodies, which we employed for immunostaining of dissected *C. elegans* germ lines [18]. We confirmed the perinuclear staining pattern we observed with a third independently generated CED-4 antibody, which specifically recognizes CED-4 (Suppl. Figure 1A,B) [18]. Using high-resolution imaging, we found that CED-4 is expressed in the entire germ line, located primarily around the nucleus with additional much weaker granular structures occurring in the cytoplasm (Figure 1A). Since the current model of apoptosis regulation depends on the direct interaction between CED-4 and mitochondrial CED-9, we next tried to establish whether CED-4 staining was associated with mitochondria as previously reported [6]. We visualized mitochondria by staining dissected germ lines with a cocktail of monoclonal antibodies recognizing conserved mitochondrial proteins. Specificity for mitochondria was confirmed by the perfect overlap of the staining patterns of the different antibodies in germ lines (Suppl. Figure 2A) as well as embryos (Suppl. Figure 2B). To our surprise we found that CED-4 does not colocalize with mitochondria in germ cells (for late pachytene cells see Figure 1A). The separate localization of CED-4 and mitochondria is most apparent when scanning through Z stacks of representative germ lines (Suppl. Movie 1, CED-4; Suppl. Movie 2, CED-4/mitochondria). We found the same non-mitochondrial staining patterns for CED-4 in mitotic, transition zone, and both early and late stage pachytene germ cells (data not shown). We confirmed the absence of CED-4 mitochondrial staining with an additional CED-4 antibody we previously generated (Suppl. Figure 1B). Finally, we transformed worms with a construct encoding for CED-4::GFP driven by the *ced-4* promoter. The fusion protein was functional,

rescuing the apoptosis defect of the *ced-4(n1162)* loss-of-function allele (Figure 2A). When we analyzed CED-4 localization in the transgenic worms using immunofluorescence with anti-GFP antibodies, we again did not see any obvious colocalization of CED-4::GFP with mitochondria (Figure 2B). The same predominantly perinuclear CED-4 localization pattern was observed following detection of the CED-4::GFP fusion protein by direct fluorescence, a finding that excludes the possibility that our staining procedures led to a loss of mitochondrial CED-4 (Figure 2C). In summary, our data show that CED-4 does not detectably localize to mitochondria in the germ line. Similarly, labelling the endoplasmic reticulum (ER) did not reveal any colocalization of the weak granular cytoplasmic CED-4 signal with the ER (Suppl. 3C). Since previous studies reporting a direct interaction of CED-9 and CED-4 at mitochondria were performed in embryos, we reasoned that our results could be explained by the existence of a fundamental difference between the regulation of developmental apoptosis and germ cell apoptosis. We therefore wished to reassess the cellular localization of CED-4 and CED-9 during embryogenesis and larval development. Using our panel of CED-4 antibodies we never saw CED-4 localized at mitochondria. In contrast to our germ line stainings we could not confirm the presence of CED-4 at nuclei with absolute certainty, due to unspecific perinuclear staining that was not present in germ lines (data not shown). We therefore analysed the same functional CED-4::GFP lines we had used for assessing the localization of CED-4 in the germ line. In agreement with our germ cell data we found no embryonic cells where CED-4::GFP staining colocalized with mitochondria, and in all cells where CED-4 was detectable it localized around the nucleus (Figure 3; Suppl. Movie 3, CED-4/mitochondria). We found the same perinculear CED-4::GFP localization by directly detecting CED-4 by GFP

fluorescence in embryos, larvae and adult worms (data not shown). Using antibodies kindly supplied by Barbara Conradt (Suppl. Figure 3A), we could confirm a partial overlap between CED-9 and mitochondria (Figure 3; Suppl. Movie 4, CED-9/mitochondria; Suppl. Movie 5, CED-4/CED-9, Suppl. Figure 3B), we were however unable to detect any overlap between CED-4 and CED-9 (Figure 3, Suppl. Movie 5, CED-4/CED-9). Imaging CED-9 in early stage embryos using deconvolution microscopy, we found that CED-9 staining was not evenly distributed along mitochondria but appeared somewhat punctate, often associated with but not perfectly overlapping with mitochondria (Suppl. Figure 3B). A punctate pattern also was observed in the germ line using the CED-9 antibody provided by the Conradt lab and the originally described CED-9 antibody (data not shown) (6). To address CED-9 localization more precisely, we employed Structured Illumination OMX microscopy, a technique that allows an approximately 2 fold higher resolution compared to conventional deconvolution microscopy [19]. Using OMX microscopy we observed a continuous staining of the inner mitochondrial membrane with anti-ATP synthase antibodies, while CED-9 staining appeared in distinct dots (Figure 4A). Zooming in on individual mitochondrial branches revealed that the CED-9 dots tend to align next to the mitochondrial inner membrane (Figure 4B, Suppl. Movie 6). This lack of overlap is consistent with OMX microscopy resolving the bulk of mitochondrial cristae that define the inner mitochondrial membrane, identified by marker proteins, from CED-9 associated with the outer mitochondrial membrane. The localization of CED-9 foci next to the mitochondrial surface became most obvious following a 3-D reconstruction of mitochondrial and CED-9 staining (Suppl. Movie 7). The CED-9 staining pattern we observed is similar to the reported staining pattern of Bcl-2 in mammalian cells [20] [21]. Unfortunately, due to technical limitations it was not

possible to triple stain nematode tissue with CED-4, CED-9 and mitochondria-specific antibodies for analysis using the OMX microscope. In summary, our results suggest that there is no fundamental difference in CED-4 localization between hermaphrodite germ cells and somatic cells, and that CED-4 localization does not overlap with mitochondria and CED-9 in the vast majority of cell types during somatic development and in the germ line. To independently confirm the localization of CED-4 and CED-9, we developed procedures to achieve subcellular fractionation (Materials and Methods). Using this procedure, and employing GAPDH as a cytosolic marker, a component of the mitochondrial ATP synthase as a mitochondrial marker and histone H2A as a nuclear marker we confirmed enrichment of the respective compartments (Figure 4C). Staining with CED-9 antibodies confirmed enrichment in the membranous fraction, while CED-4-GFP is enriched in the nuclear fraction (Figure 4C). Analogous results were obtained in independent experiments using CED-4 antibodies (data not shown). In addition, we could not find a direct interaction between CED-4 and CED-9 in co-immunprecipitation experiments and upon mass spectroscopy of CED-4 precipitates (data not shown). Intriguingly we found that CED-4 appears to colocalize with mitochondria and CED-9 in secondary spermatocytes and spermatids, cell types where apoptosis is not reported to occur [22] and where a role for CED-4 and CED-9 cell death proteins is not known (Figure 5). These cell only make out a tiny fraction of a total worm extract. This CED-4 localization in spermatocytes and spermatids, was observed with two independent CED-4 antibodies and by staining for CED-4::GFP (data not shown). In summary our combined data suggests CED-4 and CED-9 do not localize in the vast majority of cells.

We next wished to determine whether changes in CED-4 subcellular localization occur during apoptosis progression. For this, we focused our observations on the adult *C. elegans* germ line, as apoptosis can be readily induced by ionizing radiation in this tissue [23]. We and others have reported that CED-4 accumulates at the nuclear periphery of germ cells in response to ionizing radiation [18] [24]. CED-4 accumulation occurs within 6 hours of ionizing radiation and affects late pachytene as well as mitotic germ cells and transition zone nuclei (data not shown) [24] [25]. IR-dependent perinuclear accumulation of CED-4 appears strongest in late pachytene cells, which are the only germ cells competent to die by apoptosis (Figure 1B).

CED-4 perinuclear accumulation has previously been associated with apoptosis induction in *ced-9 (lf)* embryos [6]. To test if CED-4 accumulation correlates with apoptosis, we employed SIR-2.1 nuclear exclusion [18] as early stage, mitochondrial fragmentation as mid stage, and chromosome condensation as late stage cytological markers for apoptosis progression. Using high-resolution imaging we found that IR-dependent CED-4 accumulation at the nuclear periphery does not directly correlate with apoptosis. Indeed, comparing individual cells that show IR-dependent CED-4 perinuclear accumulation (marked in the right panel of Figure 1B) revealed that some cells contained intact mitochondria, as well as SIR-2.1 localized to the nucleus (cell numbered (1), Figures 1B and 6), while other cells were losing (2) or had lost nuclear SIR-2.1 (3) and contained fragmented mitochondria (3) and are thus corresponding to early to mid stage apoptotic cells (Figure 1B; Figure 6; CED-4; Suppl. Movie 8 CED-4/mitochondria; Suppl. Movie 9, CED-4/SIR-2.1;). Thus CED-4 perinuclear accumulation occurs both in healthy and in apoptotic cells. It should also be noted that

the dose of irradiation we used only leads to a two-fold reduction in egg laying, implying that a high proportion of germ cells can survive CED-4 perinuclear accumulation [23]. Only late stage corpses (4) showed evidence of chromatin fragmentation. These corpses also often showed excessive CED-4 staining (CED-4 hyper-accumulation) at the nuclear periphery and also throughout the nucleus (4). In very late stage corpses (5 and 6) chromatin had started to condense and CED-4 staining had disappeared (Figure 1B; Figure 6; Suppl. Movies 8 and 9). Thus, CED-4 hyper-accumulation seems to be a consequence of corpse degradation and only occurs in very few late stage apoptotic cells. To more precisely determine where CED-4 localizes before and after ionizing radiation we used OMX microscopy to observe CED-4 and nuclear pore complexes by immunostaining, and found that CED-4 is located outside of the nucleus before and after irradiation (Figure 1C). Unfortunately, OMX microscopy does not permit quantification of the CED-4 perinuclear accumulation in irradiated germ cells. We next wished to establish if the core apoptosis pathway is needed for CED-4 perinuclear accumulation. We analyzed an *egl-1* loss-of-function mutant as well as a *ced-9* gain-of-function mutant, both of which have dramatically reduced levels of DNA damage induced germ cell apoptosis. We found that CED-4 fails to accumulate at the nuclear periphery in response to IR in an *egl-1(lf)* as well as in a *ced-9(gf)* background (for representative pictures, see Figure 7). In contrast to this, CED-4 strongly accumulates at the nuclear periphery in *ced-9(lf); ced-3(lf)* double mutants, where apoptosis induction is triggered by the loss of CED-9 while apoptosis execution is blocked by the absence of the CED-3 caspase. Thus we confirm previous data obtained from observing embryos suggesting that the loss of CED-9 leads to CED-4 perinuclear accumulation [6], but our combined data

suggest that at least during germ cell apoptosis in wild type animals this accumulation is not sufficient for apoptosis induction.

Discussion

In summary we provide evidence that apoptosis regulation mediated by CED-4 and CED-9 is unlikely to be solely explained by a direct interaction between these two proteins. While we found colocalization of CED-4 and CED-9 at mitochondria in spermatocytes and were thereby able to confirm that the reported *in vitro* interaction between CED-4 and CED-9 indeed appears possible *in vivo*, our data clearly show that in the majority of tissues CED-4 and CED-9 do not overlap. We cannot rule out the possibility that a small undetectable fraction of CED-4 directly interacts with CED-9 in mitochondria. Alternatively a small fraction of CED-9 might be in the nucleus where it could colocalize with CED-4. We think that the CED-9 background staining in the nuclear fraction of the cell fractionation experiment is likely due to imperfect fractionation, but we cannot rule out that some CED-9 not detectable by cytology might be associated with the nucleus. Nevertheless, we clearly show that the vast majority of CED-4 is not associated with CED-9, a localization pattern that according to the current model should result in active CED-4 and initiation of apoptosis. It has been previously reported that an antiapoptotic isofom of CED-4, CED-4L exists [26]. We were not able to differentiate between the canonical CED-4 (CED-4S) and CED-4L in western blots, likely because those two isoforms only differ by 22 amino acids present in CED-4L and missing in CED-4S[26]. Given that we used polyclonal antibodies that were raised against the entire CED-4S protein we think it is highly unlikely that our staining only detect the antiapoptotic CED-4 isoform. Our data on CED-4 localization is largely based on the *C. elegans* germ line

system. Extruding germ lines generally allows for more efficient antibody penetration and staining as compared to embryos, where staining procedures require permeabilization of the egg-shell. Nevertheless, the convergence of the CED-4 localization pattern we observe by combined cytological and biochemical methods, as well as the imaging of CED-4::GFP in the germ line and during embryogenesis indicates that the localization of CED-4 does not fundamentally differ between the germ line and during development.

Our notion that apoptosis induction might not be regulated by the direct interaction between CED-4 and CED-9 is in agreement with a recent report showing that a CED-9 mutant defective in CED-4 binding is still able to rescue the embryonic lethality associated with the excessive apoptosis in a *ced-9* loss of function background [27]. As in mammals *C. elegans* apoptosis induction may require additional, as of yet unknown factors for the activation of CED-4. In mammals cytochrome c release from mitochondria is required for Apaf-1 activation. However, the missing activator of CED-4 is unlikely to be cytochrome c, as CED-4 lacks the WD40 domain needed for cytochome c binding. Furthermore, we did not observe mitochondrial release of cytochrome c in response to apoptotic stimuli (data not shown). Analogous to mammalian systems, the release of *C. elegans* AIF and EndoG from mitochondria, as well as mitochondrial fragmentation, have been implicated in *C. elegans* apoptosis induction. However, only a weak apoptosis defective phenotype is observed following depletion of AIF and EndoG [14] [13]. Nevertheless, CED-9 might have a role in regulating the release of mitochondrial proteins. The Bcl-2 family of proteins are related to bacterial pore forming proteins and Bcl-2 has been shown to be able to form pores in synthetic membranes [28] [29] [30] [15]. Furthermore, CED-9 is able to

insert into artificial membranes causing membrane permeabilization and the fusion of membrane vesicles [15]. These findings are in line with recent reports showing that CED-9 overexpression leads to the excessive fusion of mitochondrial membranes in mammalian tissue culture systems but also in various *C. elegans* tissues. In summary our results are not consistent with the widely held notion that the decision between *C. elegans* cell survival and cell death is mediated by a direct interaction of the Apaf-1-like molecule CED-4 and Bcl-2-like CED-9 *in vivo*. It will be interesting to explore how CED-9 controls CED-4 activation *in vivo* and if this relates to changes in mitochondrial permeability or dynamics.

Materials and methods

C. elegans strains:

C. elegans strains were maintained at 20°C on NGM plates and were fed with *E. coli* (OP50 strain) as described previously [31]. MT2547 *ced-4 (n1162)III*; MT7386 *ced-9 (n2812)III, ced-3(n717)IV*; MT4771 *ced-9(n1950)III*; TG1768 *egl-1(n3082)V*; TG1765 *ced-3(n717) IV*; TG1766 *ced-4(n1162) unc-119(ed3)III*; TG1767 *gt Ex[Pced-4::ced-4::gfp::ced-4utr, unc-119(+)]ced-4(n1162) unc-119(ed3).*

Antibodies:

To generate the 9104.1 rabbit anti CED-4 antiserum, 6X His-tagged CED-4 (pGA333) was used for immunization, and MBP (maltose binding protein) tagged CED-4 (pGA334) was used to purify the antibody as described by Greiss et al. [18]. The 9103.1 Rabbit CED-4 antibody and the 10147.1 Goat CED-4 antibody are described by Greiss et al. [18], anti-CED-9 antibodies are described by Rolland et al. [17].

Western blotting

Worms were lysed using a mini beadbeater (BioSpec Products) (3 X 20") set to maximum, using 0.7 mm Zirconia Beads (BioSpec Products) in 150 µl of 7 M urea lysis buffer containing 0.1 M DTT, 0.05% Triton X-100, 25 mM NaCl, 20 mM HEPES/KOH pH 7.5. The protein lysate was incubated on ice for 30 minutes followed by 20 minutes centrifugation at 13000 RPM in an Eppendorf tabletop

centribuge at 4 ºC. Total protein concentration was measured by Bradford assay (Biorad). Lysate equivalent to 10 µg of protein was separated by SDS-PAGE electrophoresis using 4-12 % gradient gels (Invitrogen). Proteins were transferred to nitrocellulose membrane using the Invitrogen iBlot system, followed by blocking with PBST (PBS supplemented with 0.1 % Tween 20) containing 5 % milk powder for 30' at RT. Probing with anti CED-9 antibody (1:1000) was performed over night at 4ºC. Washing was done at RT for 3 times for 10' each with ice cold washing buffer (PBS containing 0.1 % Tween 20). HRP conjugated donkey anti rabbit antibodies (Jackson Immunochemicals) were used as secondary antibodies at a dilution of 1:10000). Incubation was at RT.

Immunostaining and microscopy:

Germ line staining for Deltavision microscopy: Immunostaining of germ lines and imaging using Deltavision microscopy was done as described by Greiss et al., using the following antibodies and dilutions [18]. Rabbit anti CED-4 (9103.1) 1:100, rabbit anti CED-4 (9104.1) 1:200, rabbit anti CED-9 (CED-9.1) 1:150, goat anti SIR-2.1 (126.1) 1:100. Antibodies used for mitochondrial staining are described by Greiss et al. using a 1:200 dilution. Anti ATP synthase subunit α (Mitosciences, MS507,) anti cytochrome c (MSA06). Complex IV subunit 1 (MS404), Pyruvate Dehydrogenase (MSP07) ATP synthase subunit β (MS503). The ER was stained using anti HDEL SC-53472 (Santa Cruz) (1:100). The following secondary antibodies were used for detection: Alexa 488 labelled donkey anti goat (Molecular Probes) 1:200, Alexa 568 labelled donkey anti rabbit (Molecular Probes) 1:500, Alexa 647 labelled donkey anti mouse (Molecular Probes) 1:200, alexa 488 labelled goat anti mouse IgG2a antibody (Molecular Probes) 1:200, alexa 568 labelled goat anti mouse IgG1 antibody

(Molecular Probes) 1:200, alexa 647 labelled goat anti mouse IgG2b antibody (Molecular Probes) 1:200,

Embryo:

Sample preparation was done on poly-lysine (0,1% w/v, Sigma) coated super frost Plus slides (VWR International) and fixation was done as described for the germ line with the following modifications [18]: Post fixation was done at RT. Pre blocking with Image IT FX signal enhancer (Invitrogen) was done for 15 minutes. For the staining shown in Figure 2, the CED-4::GFP fusion was detected by the "GFP booster, Chromotex" anti-GFP monovalent antibody which is directly coupled to ATTO 488 fluorescent dye, and which was incubated (1:200) with the secondary antibodies in this straining. Antibodies were used at the same dilution as for the germ line staining.

Staining for SI-OMX microscope:

Embryos were prepared and fixed as described above [18] except for the permeabilization, which was done by 4 10' incubations at RT, and preblocking with Image IT FX signal enhancer (Invitrogen) which was done for 10' at RT. Primary antibodies and their dilutions were as follows: IgG2b anti ATP synthase subunit α (MS507) 1:150, IgG2a anti cytochrome c (MSA06) 1:150, CED-9.1 antibody 1:100. Secondary antibodies were as follows: alexa 568 labelled donkey anti rabbit (Molecular Probes) 1:400, alexa 488 labelled goat anti mouse IgG2a antibody (Molecular Probes) 1:150, alexa 488 labelled goat anti mouse IgG2b antibody (Molecular Probes) 1:150, DyLight 549 labelled Goat anti mouse IgG2b (Jackson

Immunochemicals) 1:100. Germ lines were fixed and stained as described above, except that germ lines were ruptured before fixation. Mouse monoclonal antibody MAb414 (1:150, Covance Research Products) was used to stain the nuclear pore complex.

Image analysis and 3D reconstruction:

Images were analyzed using softWoRx Suite and softWoRx Explorer software (AppliedPrecision). SI-OMX 3D reconstructions and subtraction of noise were performed using Imaris software (Bitplan AG, Scientific Software).

Generation of transgenic worms:

The sequence of the *ced-4::gfp* fusion plasmid (pGA402) containing *ced-4* promoter, *ced-4* genomic sequence followed by GFP inserted right before the stop codon and the *ced-4* 3'-UTR can be obtained upon request. The *ced-4* promoter and *ced-4* genomic sequences were amplified using the following primers:

GA2194: [5'TGCAGGCGCGCCCATGCTTTCGTGGTGACATTG3'] and

GA2199: [5'AAAGCGGCCGCCACAGCATGCAAAATTTTTGAG3'].

To clone the 3'-*UTR,*

GA2223a: [5'TCGAGGCCGGCCTAAAACCTATCGTGTACAATATTG] and

GA2224: [5'TCGAGGGCCCGTTCTTGCATTCGATCTTCTCAATTTG] were used.

To create transgenic lines, 5 μg of pGA402 plasmid was used to transform TG1766 *ced-4(n1162); unc-119(ed3)* worms by biolistic bombardment using a PDS-100/He particle delivery system (Bio-Rad) [32].

Subcellular fractionation:

Lysis of worms and release of cytoplasmic content. 200 µl of worm pellet (mixed stage) was used. Worms were washed 3X in M9 buffer and collected by sedimentation. Worms were resuspended in 0.2 ml ice-cold extraction buffer CE1 supplemented with protease inhibitor (Qiagen Qproteome Cell Compartment Kit). To disrupt the cuticles and to release the cells and cytoplasmic content, 100-150 µl 0.7 mm Zirconia Beads (BioSpec Products) were added to the vial, followed by bead beating (Mini-Beadbeater-8, BioSpec Products) at max speed for 3 times each 5 seconds. ~70% lysis was confirmed by microscopic observation, scoring for released nuclei. To avoid disrupting subcellular compartments worms were not frozen before lysis. To further lyse the sample and to clear the lysate from non-lysed worms and worm cuticles, the sample was passed through cell-lysate homogenizer tubes (Qiashredder, QIAGEN) and centrifuged for 2 minutes at 100 x rcf (Eppendorf cooling benchtop centrifuge). The lysate was then transferred to new homogenizer tubes and spun for 30 seconds at 100 x rcf and the precedure was repeated once more. After a final spin for 10 seconds the lysate was free from non-lysed worms and their cuticles. Subsequently subcellular fractionation was performed according to the manufacturer's instructions, but using only 20% of the recommended volumes. After fractionation the samples were incubated with 4 times their volume of acetone at -20 C for 3 hours, followed by centrifugation at 13200 RPM for 30 minutes at 4C. The supernatant was removed and the pellet was air-dried. The pellet was resuspended in 100 µl of 2% SDS and heated at 65 C for 30 minutes with occasional vortexing. Protein concentration of all the fractions was measured using the Pierce BCA protein concentration assay following the manufacturer's instructions. For western blotting 5 µg of each sample was used. Antibodies used were: anti histone H2A antibody (Abcam AB13923) 1:1000; anti ATP synthase subunit alpha antibody (Mitosciences)

1:2500; anti GAPDH antibody (Sigma G8795) 1:10000; anti GFP antibody (Cell Signalling Technology 2956) 1:1000; anti CED-9 antibody 1:2000.

Acknowledgments

Research was funded by a CR-UK CDA (C11852/A4500) award and by a Wellcome Trust senior Research fellowship (0909444/Z/09/Z) to AG. EP was supported by a CRUK PhD studentship (C11852/A8052) and SG was supported by a Wellcome Trust Project grant (081923/Z/07/Z) to AG. We are grateful to Barbara Conradt for sharing CED-9 antibodies and to Ashley Craig and Ulrike Gartner for proofreading. We also thank Magali Billet for helping with the CED-4:GFP construct, Pablo Ibanez Cruceyra for assisting with the generation of transgenic worms and Mark Larance for help, relating to establishing subcellular fractionation. We are also thankful to The Dundee CLS imaging facility and particularly wish to thank Sam Swift and Emma King for their technical support. SULSA (Scottish Universities Life Science Alliance) supported the OMX microscope.

Conflict of Interest

The authors declare that there is no financial conflict of interest.

Abbreviations list

ced: cell death abnormal

egl: egg laying defective

SI-OMX: Structural Illumination Opticam Sxperimental Microscopy

Apaf-1: Apoptotic Protease Activating Factor 1

Bcl-2: B Cell Lymphoma 2

References:

1. Ellis HM, Horvitz HR (1986) Genetic control of programmed cell death in the nematode C. elegans. Cell 44: 817-829.
2. Conradt B, Horvitz HR (1998) The C. elegans protein EGL-1 is required for programmed cell death and interacts with the Bcl-2-like protein CED-9. Cell 93: 519-529.
3. Hengartner MO, Ellis RE, Horvitz HR (1992) Caenorhabditis elegans gene ced-9 protects cells from programmed cell death. Nature 356: 494-499.
4. del Peso L, Gonzalez VM, Inohara N, Ellis RE, Nunez G (2000) Disruption of the CED-9.CED-4 complex by EGL-1 is a critical step for programmed cell death in Caenorhabditis elegans. J Biol Chem 275: 27205-27211.
5. Liu X, Kim CN, Yang J, Jemmerson R, Wang X (1996) Induction of apoptotic program in cell-free extracts: requirement for dATP and cytochrome c. Cell 86: 147-157.
6. Chen F, Hersh BM, Conradt B, Zhou Z, Riemer D, et al. (2000) Translocation of C. elegans CED-4 to nuclear membranes during programmed cell death. Science 287: 1485-1489.
7. Yang X, Chang HY, Baltimore D (1998) Essential role of CED-4 oligomerization in CED-3 activation and apoptosis. Science 281: 1355-1357.
8. Yan N, Chai J, Lee ES, Gu L, Liu Q, et al. (2005) Structure of the CED-4-CED-9 complex provides insights into programmed cell death in Caenorhabditis elegans. Nature 437: 831-837.
9. Qi S, Pang Y, Hu Q, Liu Q, Li H, et al. Crystal structure of the Caenorhabditis elegans apoptosome reveals an octameric assembly of CED-4. Cell 141: 446-457.
10. Spector MS, Desnoyers S, Hoeppner DJ, Hengartner MO (1997) Interaction between the C. elegans cell-death regulators CED-9 and CED-4. Nature 385: 653-656.
11. Chinnaiyan AM, O'Rourke K, Lane BR, Dixit VM (1997) Interaction of CED-4 with CED-3 and CED-9: a molecular framework for cell death. Science 275: 1122-1126.
12. Yan N, Xu Y, Shi Y (2006) 2:1 Stoichiometry of the CED-4-CED-9 complex and the tetrameric CED-4: insights into the regulation of CED-3 activation. Cell Cycle 5: 31-34.
13. Wang X, Yang C, Chai J, Shi Y, Xue D (2002) Mechanisms of AIF-mediated apoptotic DNA degradation in Caenorhabditis elegans. Science 298: 1587-1592.
14. Parrish J, Li L, Klotz K, Ledwich D, Wang X, et al. (2001) Mitochondrial endonuclease G is important for apoptosis in C. elegans. Nature 412: 90-94.

15. Frederick JT, Zuckerman JE, Wells RC, Hill RB The C. elegans b-cell lymphoma 2 (bcl-2) homolog cell death abnormal 9 (ced-9) associates with and remodels lipid membranes. Protein Sci.
16. Delivani P, Adrain C, Taylor RC, Duriez PJ, Martin SJ (2006) Role for CED-9 and Egl-1 as regulators of mitochondrial fission and fusion dynamics. Mol Cell 21: 761-773.
17. Rolland SG, Lu Y, David CN, Conradt B (2009) The BCL-2-like protein CED-9 of C. elegans promotes FZO-1/Mfn1,2- and EAT-3/Opa1-dependent mitochondrial fusion. J Cell Biol 186: 525-540.
18. Greiss S, Hall J, Ahmed S, Gartner A (2008) C. elegans SIR-2.1 translocation is linked to a proapoptotic pathway parallel to cep-1/p53 during DNA damage-induced apoptosis. Genes Dev 22: 2831-2842.
19. Schermelleh L, Carlton PM, Haase S, Shao L, Winoto L, et al. (2008) Subdiffraction multicolor imaging of the nuclear periphery with 3D structured illumination microscopy. Science 320: 1332-1336.
20. Hockenbery D, Nunez G, Milliman C, Schreiber RD, Korsmeyer SJ (1990) Bcl-2 is an inner mitochondrial membrane protein that blocks programmed cell death. Nature 348: 334-336.
21. Riparbelli MG, Callaini G, Tripodi SA, Cintorino M, Tosi P, et al. (1995) Localization of the Bcl-2 protein to the outer mitochondrial membrane by electron microscopy. Exp Cell Res 221: 363-369.
22. Jaramillo-Lambert A, Harigaya Y, Vitt J, Villeneuve A, Engebrecht J Meiotic Errors Activate Checkpoints that Improve Gamete Quality without Triggering Apoptosis in Male Germ Cells. Curr Biol.
23. Gartner A, Milstein S, Ahmed S, Hodgkin J, Hengartner MO (2000) A conserved checkpoint pathway mediates DNA damage--induced apoptosis and cell cycle arrest in C. elegans. Mol Cell 5: 435-443.
24. Deng X, Yin X, Allan R, Lu DD, Maurer CW, et al. (2008) Ceramide biogenesis is required for radiation-induced apoptosis in the germ line of C. elegans. Science 322: 110-115.
25. Zermati Y, Mouhamad S, Stergiou L, Besse B, Galluzzi L, et al. (2007) Nonapoptotic role for Apaf-1 in the DNA damage checkpoint. Mol Cell 28: 624-637.
26. Shaham S, Horvitz HR (1996) An alternatively spliced C. elegans ced-4 RNA encodes a novel cell death inhibitor. Cell 86: 201-208.
27. Dreze M, Charloteaux B, Milstein S, Vidalain PO, Yildirim MA, et al. (2009) 'Edgetic' perturbation of a C. elegans BCL2 ortholog. Nat Methods 6: 843-849.
28. Muchmore SW, Sattler M, Liang H, Meadows RP, Harlan JE, et al. (1996) X-ray and NMR structure of human Bcl-xL, an inhibitor of programmed cell death. Nature 381: 335-341.
29. Hengartner MO (2000) The biochemistry of apoptosis. Nature 407: 770-776.
30. Desagher S, Martinou JC (2000) Mitochondria as the central control point of apoptosis. Trends Cell Biol 10: 369-377.
31. Brenner S (1974) The genetics of Caenorhabditis elegans. Genetics 77: 71-94.
32. Praitis V, Casey E, Collar D, Austin J (2001) Creation of low-copy integrated transgenic lines in Caenorhabditis elegans. Genetics 157: 1217-1226.

Figure Legends

Figure 1) CED-4 is not localized on mitochondria in the germ line. **A)** Representative pictures of late stage pachytene germ cells were taken by Deltavision microscopy. CED-4 staining was done with the CED-4 9104.1 antibody. Mitochondria were stained with anti ATP synthase and anti cytochrome c antibodies. The corresponding 3D stacks of the images are shown in Suppl. Movie 1 (CED-4) and Suppl. Movie 2 (CED-4/mitochondia) scale bar: 6 μm. **B)** CED-4 perinuclear accumulation upon treatment with IR. A representative healthy cell, and corpses indicative of different stages of apoptosis progression are indicated in the right panel (1-6). A blow up of these cells is shown in Figure 6A. 3D representations of the pictures and various overlaps are shown in Suppl. Movies 11 and 12. Note that the CED-4 signal intensity in B is lowered by 15% compared to A, to allow for better visualization **C)** OMX microscopy of single germ cells before and after IR (CED-4 green, nuclear pore complex red). Scale bar: 4 μm

Figure 2) Perinuclear localization of CED-4::GFP. **A)** The *ced-4 gt Ex[Pced-4::ced-4::gfp::ced-4utr, unc-119(+)]* construct rescues the *ced-4(n1162)* apoptosis defect. Only worms carrying the CED-4::GFP transgene were scored. **B)** CED-4::GFP

staining using anti GFP antibodies. A white arrow indicates a very late stage corpse, where mitochondria are fragmented, chromatin is condensed and CED-4 staining is absent (see **Figure 1B**, **Figure 6**). **C)** Direct visualization of CED-4::GFP using fluorescence microscopy. Left panel DIC image of pachytene stage germ cells, right panel overlap with fluorescence image. Scale bar: 10 μm.

Figure 3) Staining of an embryo undergoing morphogenesis indicates that CED-4 does not colocalize with CED-9 and mitochondria. CED-4 is visualized using anti GFP antibodies (see Experimental Procedure). The image shown is a projection of 6 Z stacks. 3D scans are shown in Suppl. Movies 3-5. Scale bar: 10 μm

Figure 4) A) Punctate CED-9 staining is associated with mitochondria. **B)** A blow up of mitochondrial branches (indicated by arrows) is shown in the lower right panels. Scale bar: 4 μm. A 3D Scan of the picture is shown in Suppl. Movie 6. **C)** Subcellular Fractionation. Mixed stage *C. elegans* extracts were generated and fractionated as described in Materials and Methods. Enrichment of subcellular compartments was confirmed using antibodies against the indicated marker proteins.

Figure 5) CED-4 and CED-9 staining overlaps in secondary spermatocytes. The CED-4 (10147.1) antibody was used [18].

Figure 6) A**)** Various stages of germ cell apoptosis. Cells/corpses shown are indicated in Figure 1b. Scale bar: 6 μm

Figure 7) CED-4 perinculear accumulation upon IR is absent in *egl-1* loss of function and *ced-9* gain of function mutants. The CED-4 (9104.1) antibody was used. Scale bar: 10 µm.

Supplemental Information

Suppl. Figure 1) A) Characterization of the CED-4 9104.1 antibody. Antibody staining is absent in the *ced-4 (n1162)* mutants. **B)** Germ line staining with the CED-4 9103.1 antibody and the cocktail of anti-mitochondrial antibodies. Scale bar: 10 µm

Suppl. Figure 2) A) Overlap of staining pattern with multiple monoclonal antibodies against conserved mitochondrial proteins (see Experimental Procedure). Single and double stainings are shown in the upper panel. Various merges are shown in the lower panel. Scale bar: 10 µm **B)** Mitochondrial double staining of an embryo. Pictures were taken by SI-OMX microscopy. Scale bar: 5 µm.

Suppl. Figure 3) A) CED-9 Western Blot. **B)** Deconvoled image of CED-9 and mitochondrial staining of ~16 and ~32 cell stage embryos. Scale bar: 6 µm. **C)** The ER was stained using antibodies against the HDEL ER retention signalling peptide (Materials and Methods). Scale bar: 10 µm.

Suppl. Movie 1) CED-4 (red) staining of pachytene stage germ cells.

Suppl. Movie 2) CED-4 (red) and mitochondria (green) staining of pachytene stage germ cells.

Suppl. Movie 3) CED-4 (red) and mitochondria (green) staining of a late stage embryo.

Suppl. Movie 4) CED-9 (red) and mitochondria (green) staining of a late stage embryo.

Suppl. Movie 5) CED-4 (red) and CED-9 (green) staining of a late stage embryo.

Suppl. Movie 6) Movie of OMX picture showing CED-9 (red) and mitochondria (green).

Suppl. Movie 7) 3D reconstruction of OMX picture showing CED-9 (orange) and mitochondria (green).

Suppl. Movie 8) CED-4 (red) and mitochondria (green) staining of irradiated pachytene stage germ cells.

Suppl. Movie 9) CED-4 (red) and SIR-2.1 (green) staining of irradiated pachytene stage germ cells.

Figure 4:

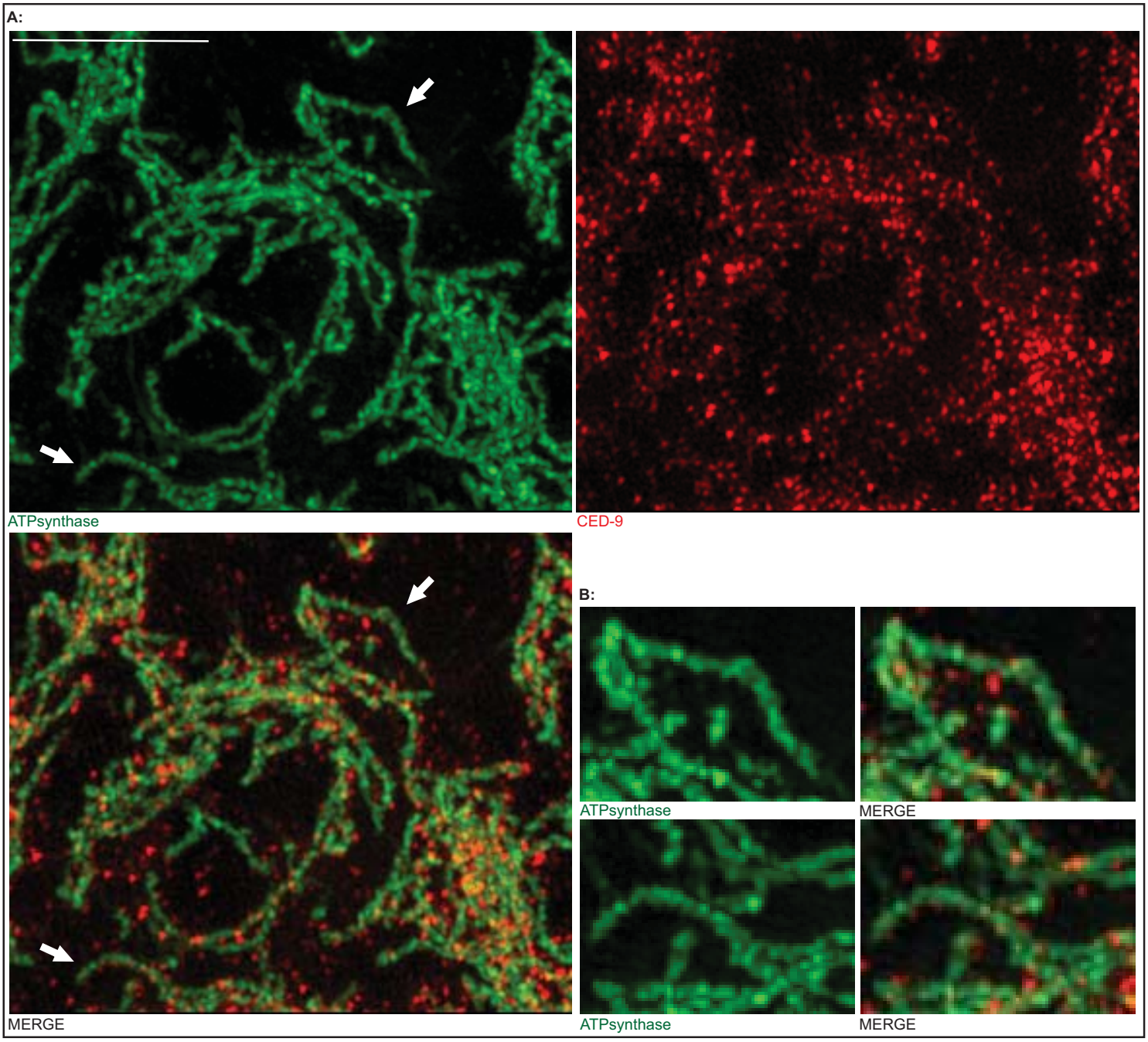
A:
ATPsynthase
CED-9
MERGE
B:
ATPsynthase
MERGE
ATPsynthase
MERGE

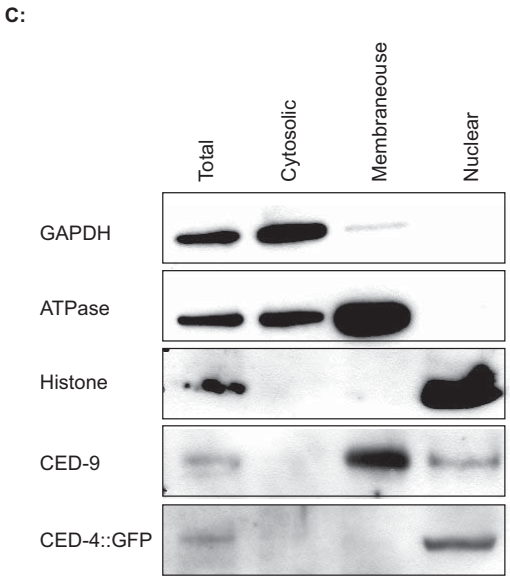
C:
Total
Cytosolic
Membraneouse
Nuclear
GAPDH
ATPase
Histone
CED-9
CED-4::GFP